High-Frequency Analysis of an Array of Line Sources on a Truncated Ground Plane

Filippo Capolino, *Member, IEEE*, Matteo Albani, *Member, IEEE*, Stefano Maci, *Member, IEEE*, and Roberto Tiberio, *Fellow, IEEE*

***Abstract*—A uniform high-frequency solution is presented for the field radiated at finite distance by a semi-infinite beam-scanning array of magnetic line sources located on a perfectly conducting half-plane. The field is represented in terms of Floquet waves plus their relevant singly and doubly diffracted rays, which arise from both the end of the array and the edge of the half-plane. This representation is uniformly valid also when transition conditions from propagating to evanescent Floquet waves occur. Furthermore, it provides a simple and attractive physical interpretation and is found numerically very effective, due to the fast convergence of the Floquet wave expansion for the field.**

***Index Terms*—Antenna arrays, electromagnetic radiation, geometrical theory of diffraction.**

I. Introduction

A UNIFORM high-frequency solution for a semi-infinite array of impressed magnetic line sources located on a perfectly electric conducting (PEC) half plane is presented in this paper. The sources have equal amplitudes, and a linear phase tapering is introduced to provide beam scanning [see Fig. 1(a)]. By invoking the localization principle of high-frequency phenomena, the uniform asymptotic solution of this canonical problem can be used to describe large finite arrays of slots on a finite ground plane, i.e., this result can be interpreted in terms of the uniform theory of diffraction (UTD) [1] description of scattering and radiation phenomena. In order to provide a physical insight and an efficient solution, a Floquet wave (FW) approach is used, which is an extension of that proposed in [2]–[5]. In particular, the field of the corresponding infinite periodic array is expanded in terms of FW, and the radiation of the actual semi-infinite array is interpreted as the superposition of traveling wave-type currents that are distributed on the semi-infinite aperture plane formed by the array sources. Each aperture distribution radiates in presence of the perfectly conducting half-plane. Since the FW series exhibits excellent convergence properties when the observation point is located away from the local surface, this representation is found more efficient than the direct summation of the spatial contributions from each element of the array, particularly when the radiation from each FW-type aperture is treated asymptotically. In this case, each contribution can be interpreted as the sum of the FW's themselves and their relevant diffraction at the edge of the aperture. Since the array is supported by a ground plane, the singly diffracted rays undergo a subsequent diffraction at its edge. In summary, as depicted in Fig. 1(b), the high-frequency description of the total radiation mechanism is given in terms of FW's, singly diffracted rays excited at the edge of the array by the incident FW's, and doubly diffracted rays excited at the edge of the half-plane by the singly diffracted grazing ray. These latter ray contributions provide an estimate of the field in the optical shadow region and ensure the continuity of the total field at those grazing aspects, where the singly diffracted field exhibits a discontinuity.

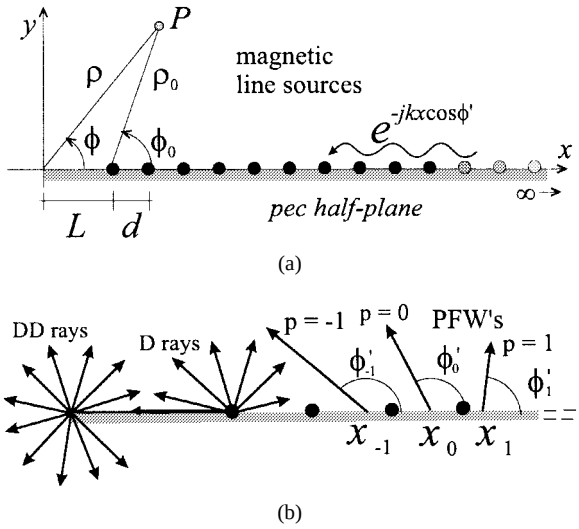

Fig. 1. (a) Geometry of the array on a semi-infinite ground plane. (b) Propagating Floquet waves (PFW$_p$, $p = 1, 0, -1$), singly diffracted (D) and doubly diffracted (DD) rays.

The high-frequency solution presented here provides a basic example for studying other problems involving double diffraction of FW's, which may occur whenever an array is located on a finite supporting structure; consequently, it provides an extension of the solutions derived in [2]–[5], which refer to arrays of line source in free-space [2]–[4] and on an infinite dielectric slab [5]. Although the model is two-dimensional, the physical picture provided by our solution can be applied to qualitatively explain the radiation by actual large array antennas, as well as the scattering by finite periodic structures of practical interest such as dichroics, polarizers, artificially hard, and soft surfaces.

Manuscript received January 21, 1997; revised November 24, 1997.

F. Capolino, M. Albani, and R. Tiberio are with the College of Engineering, University of Siena, 53100, Siena, Italy.

S. Maci is with the Department of Electronic Engineering, University of Florence, Florence, Italy.

Publisher Item Identifier S 0018-926X(98)02685-4.

This paper is organized as follows. In Section II, the problem is formulated by superimposing the near-field contributions of each source, which radiates with the Green's function of the PEC half-plane. By using a suitable spectral representation of this Green's function, the global radiation of the structure is represented in terms of a single spectral integral. In Section III, the asymptotic evaluation of this integral is carried out, leading to a uniform solution in terms of FW's and their pertinent singly and doubly diffracted rays. These latter are expressed in terms of the multiple-argument transition function derived in [6] and [7] for the double diffraction at a couple of wedges and used in [8] for describing the diffraction at a vertex of a plane angular sector. In the present case, this transition function is extended to complex values of its argument. In Section IV, the behavior of the physical mechanisms described by our solution is discussed, with particular emphasis given to the case when a transition from a propagating to an evanescent FW occurs. Numerical results are presented in Section V and compared with reference solutions.

II. Formulation

The geometry of the problem is shown in Fig. 1(a). A semi-infinite periodic distribution of magnetic current line sources with impressed amplitudes and with interelement period d are placed on a semi-infinite ground-plane. The first source is placed at a distance L from the edge of the ground plane. Two rectangular reference systems $(x,\, y)$ and $(x_0,\, y)$ are introduced with the y axis perpendicular to the plane of the array; their origins are located at the edge of the half-plane $(x = 0)$ and at the first source $(x_0 = 0)$, respectively. The relevant cylindrical reference systems are denoted by $(\rho,\, \phi)$ and $(\rho_0,\, \phi_0)$, respectively. For the sake of simplicity, but without loss of generality, a traveling wave excitation $\exp(-jknd\, \cos\, \phi')$, $(n = 0,\, 1,\, 2,\, \cdots)$ is assumed, which has a unit amplitude and linear phase in order to provide beam in direction ϕ'.

By superposing the field radiated by each line current, the magnetic z field is obtained as

$$H_z = \sum_{n=0}^{\infty} f(nd + L,\, P) e^{-jk\, \cos\, \phi' nd} \tag{1}$$

where $f(x',\, P)$ is the Green's function of a perfectly conducting half-plane at the observation point P when it is illuminated by a source placed at x'. A convenient exact representation of $f(x',\, P)$ in terms of its Fourier transform $F(k_x,\, P)$ [9], is

$$f(x',\, P) = \frac{1}{2\pi} \int_{-\infty}^{\infty} F(k_x,\, P) e^{jk_x x'}\, dk_x \tag{2}$$

where

$$F(k_x,\, P) = F^{go}(k_x,\, P) + F^{d}(k_x,\, P) \tag{3}$$

$$F^{go}(k_x,\, P) = -\frac{k}{\zeta} \frac{e^{-j\rho k_x\, \cos\, \phi - j\rho \sqrt{k^2 - k_x^2}\, \sin\, \phi}}{\sqrt{k^2 - k_x^2}} \tag{4}$$

$$F^{d}(k_x,\, P) = \frac{-k}{2\pi j \sqrt{k^2 - k_x^2}\, 2\zeta} \int_{C_\alpha} \cdot G^h(\alpha,\, \phi) e^{j\rho k_x\, \cos\, \alpha - j\rho \sqrt{k^2 - k_x^2}\, \sin\, \alpha}\, d\alpha \tag{5}$$

in which

$$G^h(\alpha,\, \phi) = -\frac{2\, \cos\left(\frac{\alpha}{2}\right) \cos\left(\frac{\phi}{2}\right)}{\cos\, \alpha + \cos\, \phi} \tag{6}$$

and $C_\alpha \equiv (-j\infty,\, \pi + j\infty)$. The term $F^{go}(k_x,\, P)$, which is the Fourier transform of a Hankel function, is associated to the geometrical optics (GO) field from the line source and its image, while the contribution $F^d(k_x,\, P)$ represents the diffracted field. A clockwise indentation of the contour around the pole $\alpha = \pi - \phi$ is assumed. The branch-cut in (3) is chosen in such a way that $\mathrm{Im}\left(\sqrt{k^2 - k_x^2}\right) < 0$ in the top Rieman sheet of the k_x complex plane.

Now, (2) is used in (1) to yield, after interchanging the order of integration and summation

$$H_z = \lim_{\epsilon \to 0+} \frac{1}{2\pi} \int_{j\,\epsilon - \infty}^{j\,\epsilon + \infty} F(k_x,\, P) e^{jk_x L} \sum_{n=0}^{\infty} \cdot e^{j(k_x - k\, \cos\, \phi')nd}\, dk_x. \tag{7}$$

In doing that, a vanishing, small positive shift (ϵ) of the integration contour is assumed; as a consequence, $|\exp[j(k_x - k\, \cos\, \phi')d]|$ is strictly less than unity, so that the sum of the series inside the integral can be evaluated in a closed form

$$H_z = \lim_{\epsilon \to 0+} \frac{1}{2\pi} \int_{j\,\epsilon - \infty}^{j\,\epsilon + \infty} F(k_x) \frac{e^{jk_x L}}{1 - e^{j(k_x - k\, \cos\, \phi')d}}\, dk_x. \tag{8}$$

It is apparent that the integrand in (8) exhibits poles in the k_x complex plane that are located at $k_{xp} = k\, \cos\, \phi' + 2\pi p/d$ [see Fig. 2(a)]. For vanishing ϵ, a clockwise indentation of the integration contour around these poles is required. The residues at these poles describe the FW's of the infinite grounded array. In particular, the poles located either inside or outside the interval $(-k,\, k)$ are associated to either propagating (PFW) or evanescent FW's (EFW), respectively. Other improper poles are located on the bottom Rieman sheet $\left[\mathrm{Im}\left(\sqrt{k^2 - k_x^2}\right) < 0\right]$; although these latter poles have no physical meaning since they would describe waves that grow along the positive y axis, their presence affects the integration and need to be accounted for in the asymptotic evaluation of (8).

By using (3) in (5), and introducing the change of variable $\cos\, \alpha' = -k_x/k$, we obtain

$$H_z = H_z^{\mathrm{FW+d}} + H_z^{dd} \tag{9}$$

in which

$$H_z^{\mathrm{FW}+d} = \frac{-k}{4\pi\zeta} \int_{C_{\alpha'}} 2\, e^{jk\rho_0\, \cos(\alpha' + \phi_0)} B(\alpha',\, \phi')\, d\alpha' \tag{10}$$

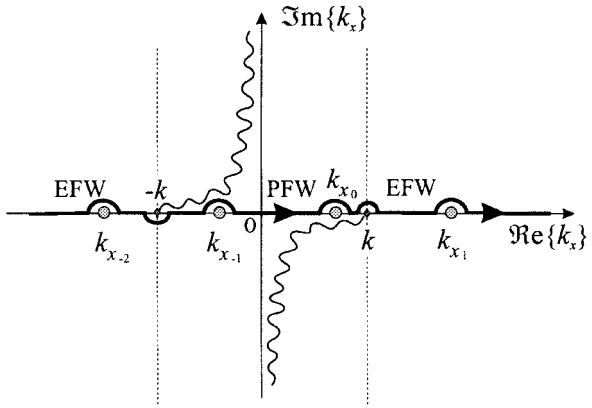

(a)

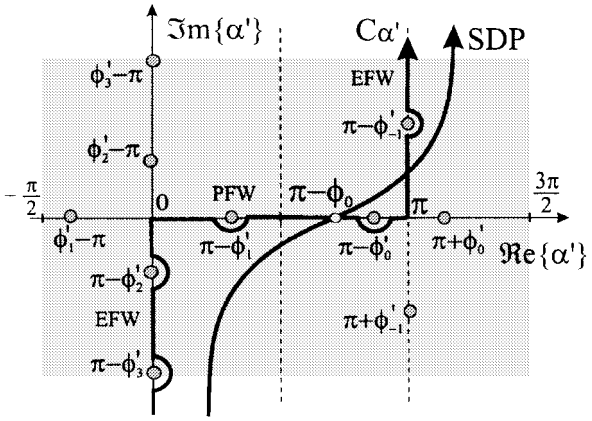

(b)

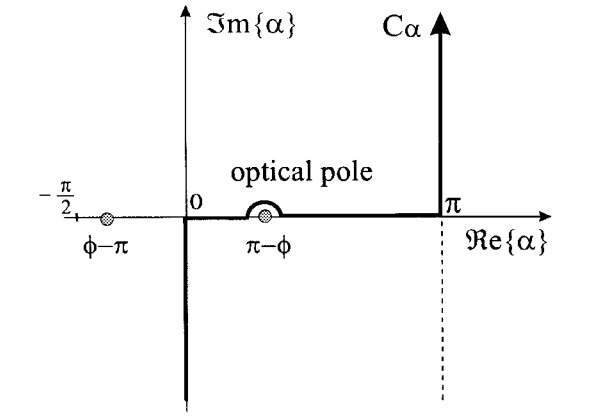

(c)

Fig. 2. (a) Complex k_z plane. (b) Complex α' plane; the shadowed region denotes the one where the poles are extracted in the asymptotic procedure ($P = 3$). (c) Complex α plane.

$$H_z^{dd} = \frac{-k}{8j\pi^2\zeta} \int_{C_\alpha} \int_{C_{\alpha'}} e^{-jkR(\alpha',\,\alpha)} B(\alpha',\,\phi') \cdot G^h(\alpha,\,\phi)\, d\alpha d\,\alpha' \tag{11}$$

where

$$R(\alpha', \alpha) = L\,\cos\,\alpha' + \rho\,\cos(\alpha - \alpha') \tag{12}$$

and

$$B(\alpha',\,\phi') = \frac{1}{1 - e^{-jkd(\cos\,\alpha' + \cos\,\phi')}}. \tag{13}$$

The contour $C_{\alpha'} \equiv (-j\infty,\, \pi + j\infty)$ detours the poles at $\pi - \phi'_p$ counterclockwise [see Fig. 2(b)], while the contour $C_\alpha \equiv (-j\infty,\, \pi + j\infty)$ detours the pole at $\pi - \phi$ clockwise [see Fig. 2(c)]. Also in (10), the identity

$$\rho_0\,\cos(\alpha' + \phi_0) = (\rho\,\cos\,\phi - L)\,\cos\,\alpha' - \rho\,\sin\,\phi\,\sin\,\alpha' \tag{14}$$

has been used. The integral representations for $H_z^{\mathrm{FW}+d}$ and H_z^{dd} arise from $F^{go}(k_x,\, P)$ and $F^d(k_x,\, P)$, respectively. As a consequence, the contribution $H_z^{\mathrm{FW}+d}$ asymptotically leads to the sum of the FW contributions and their diffraction at the end of the array and H_z^{dd} to the double diffraction contribution. Expressions (10) and (11) are well suited for their asymptotic evaluation, which will be discussed in the next section.

III. High-Frequency Representation

The integrand in (11) exhibits separated poles in the two variables of integration. In particular, one pole occurs at $\pi - \phi$ in the α complex plane, while an infinite number of poles occur in the α' complex plane at $\pi - \phi'_p$, being $\phi'_p = \cos^{-1}(\cos\,\phi' + 2\pi p/kd)$. As shown in Fig. 2(b), they are located along the $C_{\alpha'}$ path and correspond to the poles located on the top Rieman sheet of the complex k_x plane. The poles on the real and imaginary portions of $C_{\alpha'}$ are associated to PFW and EFW, respectively. Other improper (nonphysical) poles are distributed along loci that are equal to $C_{\alpha'}$ except for a translation of $m\pi (m = \pm 1, \pm 2, \cdots)$; these poles correspond to those on the improper Rieman sheet of the k_x plane. The asymptotic evaluations of $H_z^{\mathrm{FW}+d}$ and H_z^{dd} are presented in Appendexes A and B, respectively. In particular, $H_z^{\mathrm{FW}+d}$ is asymptotically evaluated by using the Van der Waerden method of the steepest descent [10]. To this end a convenient singularity extraction procedure is used in (10). The same procedure is adopted for the integral in (11), and a stationary phase approximation at $(\alpha',\, \alpha) = (0,\, 0)$ is applied to its resulting expression.

Eventually, the desired uniform, high-frequency representation is obtained as

$$H_z = H_z^{\mathrm{FW}} + H_z^d + H_z^{dd} \tag{15}$$

where

$$H_z^{\mathrm{FW}} = \frac{-1}{d\zeta} \sum_{p=-\infty}^{\infty} \frac{e^{-j\,k\rho_0\,\cos(\phi_0 - \phi'_p)}}{\sin\,\phi'_p}\, U(\phi_p^{sb} - \phi_0) \tag{16}$$

where we have (17) and (18), as shown at the bottom of the next page, $\epsilon_p = \mathrm{sgn}[\cos(\phi'_p)]$, $U(x)$ is the Heavyside unit step function, and

$$\phi_p^{sb} = \mathrm{Re}(\phi'_p) - tg^{-1}\{\sinh[\mathrm{Im}(\phi'_p)]\} \tag{19}$$

$$F(y) = 2j\sqrt{y}\,e^{jy} \int_{\sqrt{y}}^{\infty} e^{-jt^2}\,dt; \qquad -\frac{3\pi}{2} < \arg(y) \le \frac{\pi}{2}. \tag{20}$$

Equation (20) is the transition function of UTD [1], and $\tilde{T}(a,\, b\,w)$ is the transition function introduced in [6] and [7];

for the sake of convenience its definition is given in Appendix B. The arguments of the transition functions are

$$\delta_{p\pm} = \sqrt{2k\rho_0}\,\sin\left(\frac{\phi'_p \pm \phi_0}{2}\right) \tag{21}$$

$$a = \sqrt{2k\,\frac{\rho L}{\rho + L}}\,\cos\frac{\phi}{2}; \qquad b_p = \sqrt{2kL}\,\cos\frac{\phi'_p}{2} \tag{22}$$

$$w = \sqrt{\rho/(\rho + L)}. \tag{23}$$

The integer P is determined by the number of poles that are extracted in the asymptotic procedure, and its value in practical applications is suggested in Appendix A. It is worth noting that each EFW is attenuated in the y direction so that only few modes significantly contribute to the field for $y > 0$. However, when approaching grazing ($\phi = 0$), all the FW's are captured in the steepest descent path (SDP) deformation; thus, an infinite number of nonattenuated FW's should be considered in (16). Nevertheless, even in this case it is seen that few modes need to be retained in (16), unless the observation point is very close to a line source.

Both the singly and the doubly diffracted fields obtained from the above formulation are found accurate also under critical circumstances, as will be discussed in the next section.

IV. Behavior of the Solution

A ray picture of the contributions of FW's and singly and doubly diffracted fields is shown in Fig. 3 for different locations of the observation point P. In particular, the PFW-ray arises from a point x_p of the array and propagates along the direction ϕ'_p. It corresponds to the stationary phase point contribution of the FW-type aperture radiation integral. The above radiation integral can rigorously be obtained by applying to (1) the Poisson summation formula as shown in [2] and [3]. In this type of description, the end-point of the same radiation integral provides the singly diffracted rays H_z^d, which arise from the line source at the boundary of the array. These rays provide the continuity for both PFW's and EFW's at the shadow boundaries (SB's), which occur at $\phi_0 = \phi_p^{sb}$ (19). The SB's occur at $\phi_0 = \phi'_p$ for PFW [see Fig. 3]. Doubly diffracted rays arise from the edge of the half-plane and provide a uniform description of the field across $\phi_0 = \pi$, where the single diffracted field exhibits a discontinuity due to its GO shadowing. In the following, the behavior of the SB's and their transition regions is discussed as the phase velocity of the feeding wave changes (i.e., changing the beam pointing—Section IV-A). Some considerations are also carried out on the transition from PFW to EFW and its relationship with scan blindness phenomenon (Section IV-B).

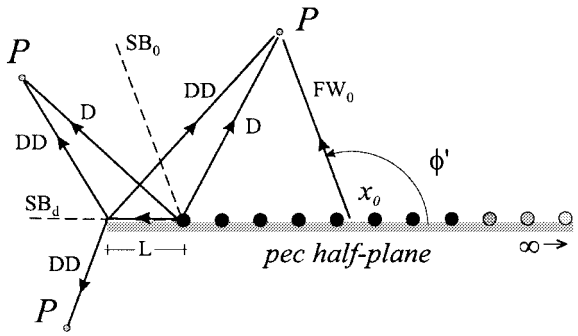

Fig. 3. High-frequency ray contributions for observation point in different regions.

A. SB's and Spatial Transition Regions

For the sake of simplicity, let us consider only one PFW. Its SB occurs at $\phi = \phi'_p$ and corresponds to the case when the stationary phase point merges with the end-point of the array [see Fig. 3]. Close to this SB, the diffracted field H_z^d exhibits a parabolic-shaped transition region [see Fig. 4(a)] in which its ray behavior changes from cylindrical to plane wave to compensate for the discontinuity of the PFW. Next, let us consider the case when the phase velocity of the feeding wave becomes slower. Actually, this occurs when scanning the beam of the array. As a consequence, the pointing angle ϕ'_p of the PFW, as well as its SB, moves toward grazing aspects and precisely reaches $\phi = \pi$ when the PFW phase velocity equals the speed of light. At this point, a further change of the scan conditions causes a transition from PFW to EFW; this corresponds to a FW pole that moves around the knee at $\alpha' = 0$ of the contour depicted in Fig. 2(b) and turns from real to imaginary. Furthermore, the transition region of the singly diffracted field degenerates from a parabola into an ellipse [see Fig. 4(b)], which is the typical shape of the transition region of the diffracted field excited by an evanescent wave [11]. This condition is referred to as the cutoff transition of the PFW and will be discussed in the next subsection.

As the phase velocity of the EFW further decreases, its SB moves from grazing aspects toward a direction perpendicular to the plane of the array, according to (19). In this direction, the traveling wave phase of the EFW matches that of the

$$H_z^d \sim U(\pi - \phi_0)\,\frac{\sqrt{k}\,e^{-jk\rho_0}}{j\zeta\sqrt{2\pi j\rho_0}}\left\{B(\pi - \phi_0,\,\phi') - \sum_{p=-P}^{P}\frac{1}{2jkd\,\sin\,\phi'_p}\left[\frac{F(\delta_{p-}^2) - 1}{\sin\left(\dfrac{\phi'_p - \phi_0}{2}\right)} + \epsilon_p\,\frac{F(\delta_{p+}^2) - 1}{\sin\left(\dfrac{\phi'_p + \phi_0}{2}\right)}\right]\right\} \tag{17}$$

$$H_z^{dd} \sim \frac{e^{-jk(\rho+L)}}{4\pi\zeta\sqrt{\rho L}\,\cos\dfrac{\phi}{2}}\left[B(0,\,\phi')F(a^2) + \sum_{p=-P}^{P}(1 - \epsilon_p)\,\frac{\tilde{T}(a,\,b_p,\,w) - F(a^2)}{2jkd\,\sin\,\phi'_p\,\cos\left(\dfrac{\phi'_p}{2}\right)}\right] \tag{18}$$

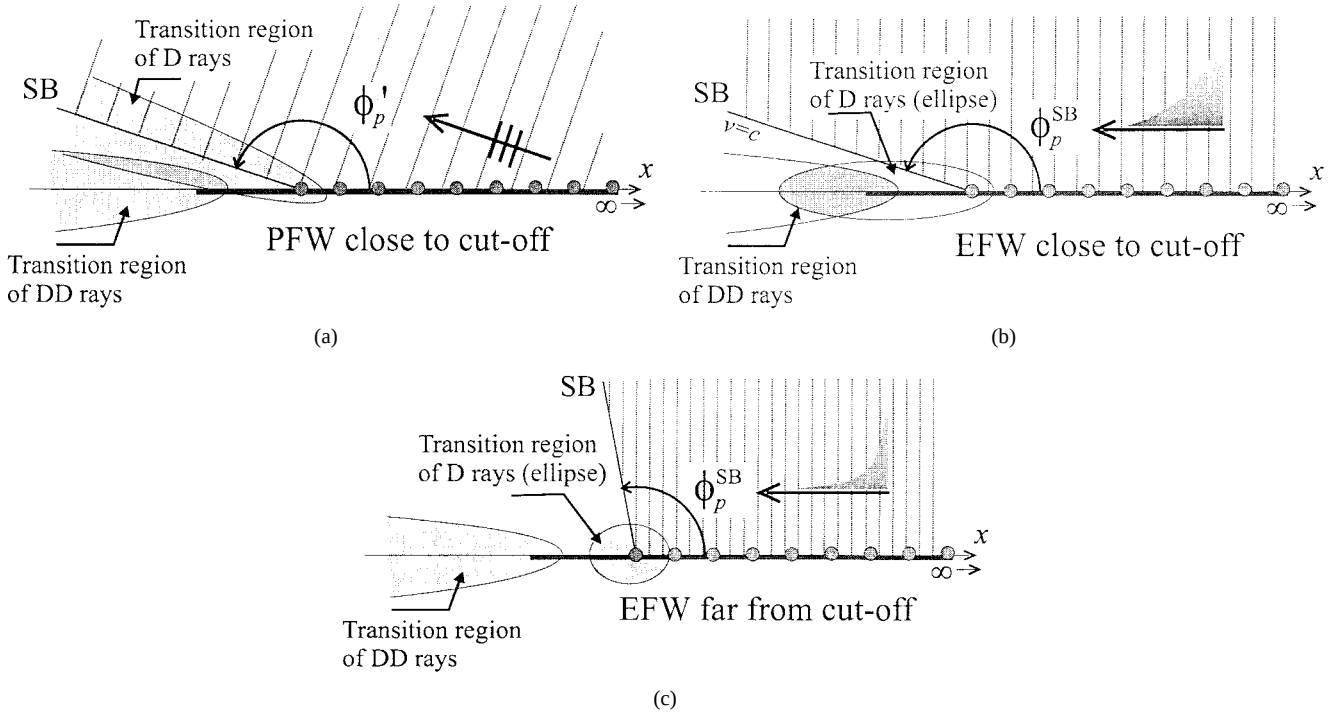

Fig. 4. Behavior of the FW shadow boundary and of the spatial transition regions of the diffracted rays during the evolution from PFW to EFW due to a beam scanning. (a) PFW close to cutoff, (b) EFW close to cutoff, and (c) EFW far from cutoff.

singly diffracted ray; i.e., the speed of light. As the speed of the feeding wave further decreases, the eccentricity of the elliptical transition region decreases too.

The SB of the singly diffracted ray (SB_d) always occurs at grazing, and the relevant transition region of the doubly diffracted field always exhibits a parabolic shape. During the cutoff transition shown in Fig. 4(a) and (b), the transition regions of the singly and doubly diffracted fields overlap. In these conditions, the transition function $\tilde{T}(a, b_p, w)$ provides a uniform description of the field by changing its parameter b_p from real to complex. When the FW is deeply evanescent so that its elliptical transition region has a small eccentricity [see Fig. 4(c)], the edge of the ground plane is practically illuminated by a ray-optical field. From a mathematical point of view, this means that $|b_p|$ becomes so large that $\tilde{T}(a, b_p, w)$ tends to $F(a^2)$ [see (40) in Appendix B]; consequently, the first term in (18), which does not contain any transition function, is asymptotically dominant. This same circumstance also occurs when the FW is propagating and SB is very far from the grazing aspect. Actually, the second term in (18) is important only during the cutoff transition of a FW. This transition and its relationship with the scan-blindness phenomenon is examined in the next subsection.

B. Cutoff Transition and Scan Blindness Phenomenon

As mentioned above, the cutoff condition of a FW corresponds to its transition from propagating to evanescent wave and may occur while changing ϕ' as well as the operating frequency. This terminology resembles the familiar cutoff condition occurring in modal waveguide propagation. Indeed, an infinite array may be modeled by a waveguide perpendicular to the plane of the array. This waveguide includes one element of the array, and the field contributions from the other elements arise from multiple reflections on its walls.

At the cutoff condition, the phase velocity of the FW matches the speed of light; consequently, the fields radiated by all the sources coherently superimpose at grazing aspect. In this case, the total radiated field tends to coherently refeed the elements, thus establishing a sort of resonance of the entire array. For an infinite number of sources that are fed by enforced currents, the field at the cutoff condition diverges, as it happens in a cavity which is fed at a resonant frequency by a time-harmonic ideal generator. In practice, at that pointing-angle where a Floquet mode meets the cutoff condition, the input impedance becomes strongly reactive so that an abrupt mismatch of the active input impedance occurs. This phenomenon is typically known as scan-blindness. When the array is semi-infinite, again the field close to the cutoff condition of the FW tends to diverge. Also, its relevant singly diffracted field becomes infinite at grazing aspect. For a finite size array at cutoff (scan-blindness), two singly diffracted fields with infinite amplitude at grazing arise from the two end points; however, their summation provides a finite, well-behaved field everywhere, as will be shown by the numerical examples in the next section.

V. Numerical Examples

Numerical calculations have been carried out to test the accuracy of the asymptotic solution, as well as to highlight the effects of the cutoff transitions. A reference solution is constructed by summing GO and UTD contributions from the sources.

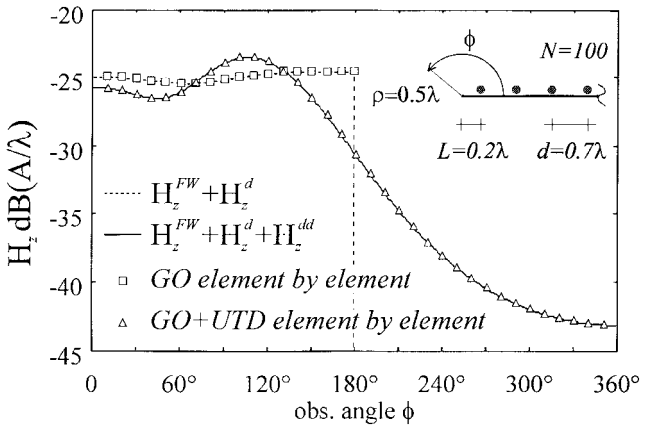

Fig. 5. Amplitude of H_z at $\rho = 0.5\lambda$ for an array of 100 lines sources ($\phi' = 150°$, $d = 0.7\lambda$, $L = 0.4\lambda$).

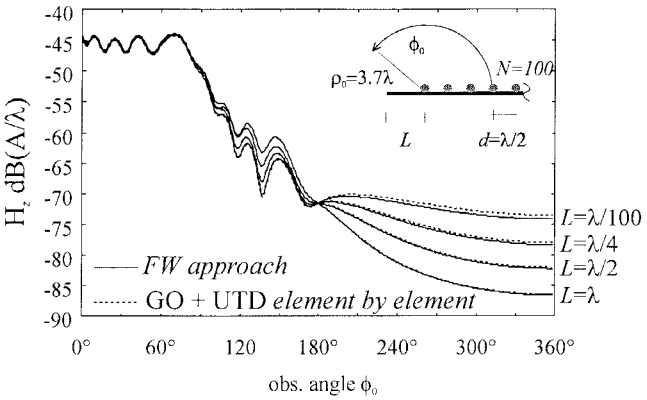

Fig. 6. Amplitude of H_z at $\rho_0 = 3.7\lambda$ for an array of 100 line sources ($d = 0.5\lambda$, $\phi' = 90°$), for various values of L; $H_z^{\mathrm{FW}} + H_z^d + H_z^{dd}$ (continuous line); reference solution (dashed line).

A near field scan at $\rho = 0.5\lambda$ is shown in Fig. 5 for an array of 100 elements with $d = 0.7\lambda$, over a semi-infinite ground plane with $L = 0.2\lambda$. The geometry is shown in the inset. The FW-approach also includes the single diffraction contribution arising from the far-out end-point of the array. Dashed and continuous lines are used to plot $H_z^{\mathrm{FW}} + H_z^d$ and $H_z^{\mathrm{FW}} + H_z^d + H_z^{dd}$, respectively. Reference solutions are also presented in this figure; these latter are obtained by superimposing either the GO fields from each source (squares) or the GO + UTD diffracted fields from each source (triangles). An angle $\phi' = 64.6°$ has been chosen for the traveling wave excitation so that the $p = -1$ FW is precisely at its cutoff condition. As mentioned in the previous section, this condition is the most critical to be described in terms of FW's since it involves a transition function with complex argument. In spite of this circumstance and of the small distance between the observation point and the edge, an excellent agreement is obtained with the reference solution, which is of course not affected by the same difficulty. It is worth noting that the computer time required by our solution is independent of the number of sources of the array; thus, it is found particularly convenient, with respect to the spatial summation, for large arrays.

In Fig. 6 the amplitude of H_z field is plotted for an array of 100 elements with $d = 0.5\lambda$ and $\phi' = 90°$. The field is

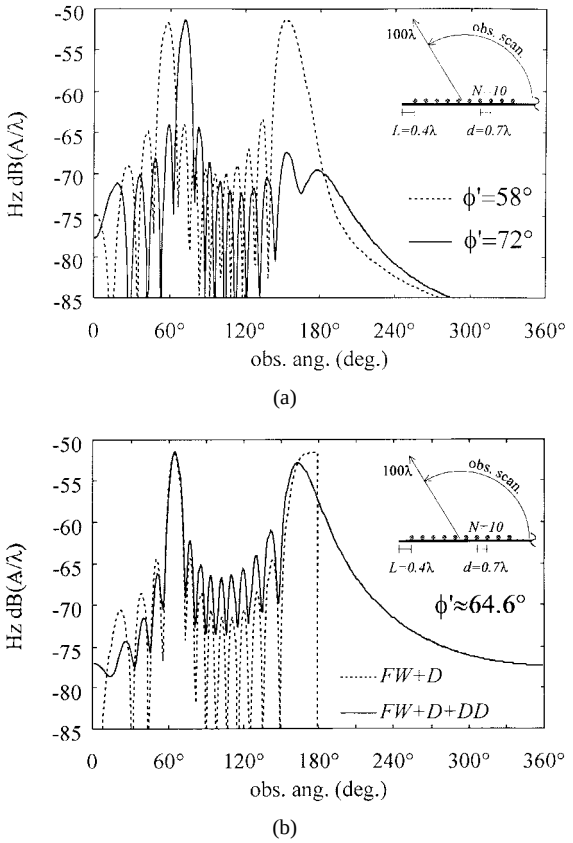

Fig. 7. Amplitude of H_z for an array of ten line sources at 100λ from the center of the array ($d = 0.5\lambda$, $L = 0.8\lambda$): (a) total field for $\phi' = 72°$ (continuous line), and $\phi' = 58°$ (dashed line) and (b) $H_z^{\mathrm{FW}} + H_z^d$ (dashed line) $H_z^{\mathrm{FW}} + H_z^d + H_z^{dd}$ (solid line) for $\phi' = 64.6°$.

observed at $\rho_0 = 3.7\lambda$ from the edge of the array. Calculations are presented for different spacings L between the edge of the array and that of the ground, such as $\lambda, 0.5\lambda, 0.25\lambda, 0.01\lambda$. An excellent agreement is found between ours (continuous line) and the reference solution (dashed line), even for $L = 0.01\lambda$, thus emphasizing the robustness of our asymptotic evaluation.

Fig. 7(a) shows the H_z field from an array of 10 sources ($d = 0.7\lambda$, observation scan at 100λ from the center of array) over a semi-infinite ground plane with $L = 0.4\lambda$. Two different phasings are considered, namely either $\phi' = 58°$ or $\phi' = 72°$, for which the same FW is either propagating or evanescent, respectively; however, in both cases it is close to the cutoff condition. It is seen that even a small change in the phase angle may cause significant differences in the radiation pattern close to grazing aspects, as expected. Results just at the cutoff condition $\phi' = 64.6°$ are shown in Fig. 7(b), where both $H_z^{\mathrm{FW}} + H_z^d$ (dashed line) and $H_z^{\mathrm{FW}} + H_z^d + H_z^{dd}$ (continuous line) are presented. In comparing Fig. 7(b) with Fig. 7(a), a more pronounced lobe at grazing is noted; also, a higher level is found for the field in the shadow region (lower half-space) and for the lobes between the two peaks. It is worth pointing out that the various results are obtained by assuming the same amplitude of the magnetic line sources. In a practical experiment, a strong impedance mismatch would occur at the cutoff condition (scan-blindness). In any case, assuming that the array is somehow fed, it is seen that a relevant part of the

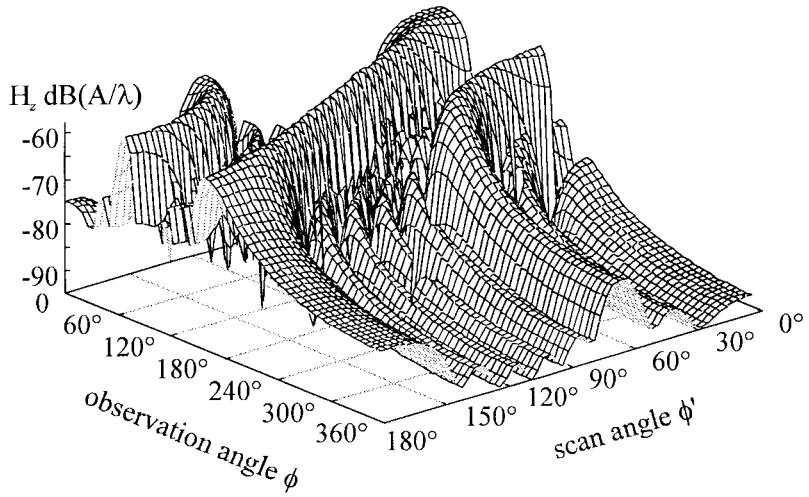

Fig. 8. Amplitude of H_z versus ϕ' and ϕ at a distance of 100λ from the center an array of six sources placed on a truncated ground plane ($d = 0.7\lambda, L = 0.4\lambda$).

power is subtracted from the main lobe and radiated in the grazing lobe. In comparing the total field (continuous line) with the field without doubly diffracted contribution, it is seen that the doubly diffracted contribution, while eliminating the discontinuity, provides a redistribution of energy that is noticeable not only in the lower half-space, but also in a wide angular range of the upper half-space.

Fig. 8 shows the field H_z radiated by an array of six sources ($d = 0.7\lambda$, $\rho = 100\lambda$ from the center of array) over a semi-infinite ground plane ($L = 0.4\lambda$) as a function of both ϕ and ϕ'. Each plane-cut perpendicular to the ϕ' axis provides a pattern similar to those in Fig. 7; the maximum value of each cut corresponds to the radiation peak of a Floquet mode that is shifted depending on ϕ'. Plane-cuts perpendicular to the ϕ-axis show the behavior of the field at each observation aspect when changing the array phasing. As expected, at aspects below the array plane, these plane-cuts exhibit a maximum for $\phi' = 64.6°$, where the cutoff condition of the $p = -1$ FW occurs.

VI. Concluding Remarks

A uniform high-frequency solution is presented for a semi-infinite beam-scanning array of magnetic line sources located on a perfectly conducting half-plane. The field is represented in terms of FW's and their relevant singly and doubly diffracted fields. This representation is uniformly valid even when the cutoff condition from propagating to evanescent FW's occurs so that it provides a neat physical description of the scan-blindness phenomenon. In order to describe this cutoff transition, an appropriate transition function is introduced by extending to complex arguments the same transition function which was previously obtained in problems involving double diffraction at a couple of perfectly conducting wedges. Although the model presented here is two-dimensional, the physical picture provided by this solution can be applied to qualitatively explain the radiation by more complex antenna arrays in a finite ground plane (e.g., slotted waveguide arrays). Furthermore, our formulation can be directly applied to find an integral representation of the electromagnetic field in the three-dimensional case; regardless, this latter situation requires a more involved asymptotic evaluation, which is presently under investigation [12]. Finally, it should be noted that the active Green's function of an array of sources is the basic block to construct the numerical Method of Moment (MoM) solution of large array antennas that may overcome problems of large matrix inversion associated to an element-by-element approach. In this regard, it should be mentioned that the field representation in terms of Floquet-wave diffracted rays can be usefully employed to expand the unknown currents of the integral equation pertinent to the array problem. This leads to the hybrid asymptotic-MoM method for large arrays described in [13].

Appendix A

In order to asymptotically evaluate the integral representation (10) of $H_z^{\mathrm{FW}+d}$, the path of integration is deformed into the SDP through the saddle point $\alpha' = \pi - \phi_0$, as shown in Fig. 2(b). The residues of the poles that are captured in this deformation represent PFW's and EFW's. This yields

$$H_z^{\mathrm{FW}+d} = H_z^{\mathrm{FW}} + H_z^d \tag{24}$$

where H_z^{FW} is the same as that defined in (15) and

$$H_z^d = \frac{-k}{2\pi\zeta} \int_{SDP(\pi-\phi_0)} e^{jk\rho_0 \cos(\alpha'+\phi_0)} B(\alpha',\, \phi')\, d\alpha'. \tag{25}$$

Next, the integral on the SDP is evaluated by the Van der Waerden method, by adding and subtracting an appropriate spectral function $W(\alpha',\, \phi')$. A convenient expression of $W(\alpha',\, \phi')$ is

$$W(\alpha',\, \phi') = \frac{1}{jk2d \sin\, \phi_p'} \sum_{p=-P}^{P} (1+\epsilon_p) G^s(\alpha',\, \phi_p') + (1-\epsilon_p) G^h(\alpha',\, \phi_p') \tag{26}$$

in which $\epsilon_p = \mathrm{sgn}(\cos\, \phi_p')$, where $G^h(\alpha,\, \phi)$ is the spectrum of the half-plane Green's function with hard boundary conditions,

which is defined in (6), and

$$G^s(\alpha,\,\phi) = -\frac{2\,\sin\left(\frac{\alpha}{2}\right)\,\sin\left(\frac{\phi}{2}\right)}{\cos\alpha+\cos\phi} \tag{27}$$

is the spectrum for the same half-plane with soft boundary conditions. This function is constructed in such a way as to have the same residues of $B(\alpha',\,\phi')$ in the region $\mathrm{Im}(\phi'_{-P}) < \mathrm{Im}\,\alpha' < \mathrm{Im}(\phi'_P)$, and $-(\pi/2) < \mathrm{Re}\,\alpha' < (3/2)\pi$, which is shadowed in Fig. 2(b) for the case $P = 3$. Increasing the number P of the poles that are extracted broadens the region in which the function $B - W$ is free of pole and improves the accuracy of the asymptotic evaluation.

The number P is chosen according to

$$P = \frac{\lambda}{d}\left[\frac{\eta}{2k\rho_0}+1+\sqrt{\left(\frac{\eta}{2k\rho_0}\right)^2+1}\right]. \tag{28}$$

This choice ensures that the jump discontinuity of the first EFW which is nonuniformly compensated by the diffracted field is proportional to $\exp(-\eta)$ when crossing its SB. In the numerical calculation, we have chosen $\eta = 10$. It is worth noting that one needs to extract not only those poles associated to physical PFW's and EFW's, but also those relevant to improper waves.

Adding and subtracting the function W in the integral yields

$$\begin{aligned} H_z^d = {} & \frac{-k}{2\pi\zeta}\int_{SDP(\pi-\phi_0)} e^{jk\rho_0\,\cos(\alpha'+\phi_0)} \\ & \times\left[B(\alpha',\,\phi')-W(\alpha',\,\phi')\right]d\alpha' \\ & + \frac{-k}{2\pi\zeta}\int_{SDP(\pi-\phi_0)} e^{jk\rho_0(\alpha'+\phi_0)}W(\alpha',\,\phi')\,d\alpha'. \end{aligned} \tag{29}$$

In the first integrand of (29), no pole occurs close to the saddle point, thus its slowly varying part is replaced by its value at the saddle point. The second integral in (29) is evaluated in an exact closed form in terms of Fresnel integral. This leads to (17).

APPENDIX B

Integral representation (11) of H_z^{dd} has a stationary phase point at $(\alpha',\,\alpha) = (0,\,0)$ and exhibits separated poles in the two variables. Its asymptotic evaluation is performed by adding and subtracting to the integrand the same function W. This yields

$$H_z^{dd} = \frac{-k}{8j\pi^2\zeta}\,(I_1+I_2) \tag{30}$$

where

$$\begin{aligned} I_1 = {} & \left[B(0,\,\phi')-W(0,\,\phi')\right]\int_{C_\alpha}\int_{C_{\alpha'}} G^h(\alpha,\,\phi) \\ & \cdot\, e^{-jkR(\alpha',\,\alpha)}\,d\alpha'\,d\alpha \end{aligned} \tag{31}$$

and

$$I_2 = \int_{C_\alpha}\int_{C_{\alpha'}} W(\alpha',\,\phi')G^h(\alpha,\,\phi)e^{-jkR(\alpha',\,\alpha)}\,d\alpha'\,d\alpha. \tag{32}$$

In (31) the slowly varying part of the integrand which depends on α' has been evaluated at $\alpha' = 0$, since no pole occurs close to zero. According to (27), an explicit expression for (32) is

$$I_2 = \frac{1}{jk2d\,\sin\,\phi'_p}\sum_{p=-P}^{P}(1+\epsilon_p)I_p^s + (1-\epsilon_p)I_p^h \tag{33}$$

in which

$$I_p^{h,s} = \int_{C_\alpha}\int_{C_{\alpha'}} G^{h,s}(\alpha',\,\phi'_p)G^h(\alpha,\,\phi)e^{-jkR(\alpha',\,\alpha)}\,d\alpha'\,d\alpha. \tag{34}$$

It is seen that $I_p^s = 0$, while I_p^h has the same form as that of the integral treated in [6]. Thus, the same asymptotic evaluation as that in [6] is applied to yield

$$I_p^h \sim 2\pi G^h(0,\,\phi')G^h(0,\,\phi)\,\frac{e^{-jk(L+\rho)}}{jk\,\sqrt{\rho L}}\,\tilde{T}(a,\,b_p,\,w) \tag{35}$$

where the transition function

$$\begin{aligned} \tilde{T}(a,\,b,\,w) = {} & \frac{a^2b^2}{j\pi(1-w^2)^{3/2}}\int_{-\infty}^{\infty}\int_{-\infty}^{\infty} \\ & \cdot\,\frac{e^{j(\xi^2+2w\xi\eta+\eta^2)}}{\left(\xi^2-\frac{a^2}{1-w^2}\right)\left(\eta^2-\frac{b^2}{1-w^2}\right)}\,d\xi\,d\eta \end{aligned} \tag{36}$$

is the same as that introduced in [6] and [7]. A convenient expression for (36) which is suitable for numerical calculations is

$$\begin{aligned} & \tilde{T}(a,\,b,\,w) \\ & \quad = \frac{2\pi jab}{\sqrt{1-w^2}}\left[\mathcal{G}\left(a,\,\frac{b+wa}{\sqrt{1-w^2}}+\mathcal{G}\left(b,\,\frac{a+wb}{\sqrt{1-w^2}}\right)\right)\right. \\ & \qquad \left.+\mathcal{G}\left(a,\,\frac{b-wa}{\sqrt{1-w^2}}\right)+\mathcal{G}\left(b,\,\frac{a-wb}{\sqrt{1-w^2}}\right)\right] \end{aligned} \tag{37}$$

where $\mathcal{G}$ is the generalized Fresnel integral [14]

$$\mathcal{G}(x,\,y) = \frac{y}{2\pi}\,e^{jx^2}\int_x^\infty \frac{e^{-j\tau^2}}{\tau^2+y^2}\,d\tau \tag{38}$$

which may efficiently be calculated as suggested in [15].

The integrand in (31) exhibits poles in only one variable and may be treated as a special case of (34). A convenient asymptotic expression for (31) can be obtained by (37) in the limit for $b \to \infty$; i.e.,

$$\begin{aligned} I_1 \sim {} & 2\pi\,\frac{e^{-jk(L+\rho)}}{jk\,\sqrt{\rho L}}\left[B(0,\,\phi')-W(0,\,\phi')\right] \\ & \times G^h(0,\,\phi)\tilde{T}(a,\,\infty,\,w) \end{aligned} \tag{39}$$

in which

$$\begin{aligned} \tilde{T}(a,\,\infty,\,w) = {} & \lim_{b\to\infty}\tilde{T}(a,\,b\,w) \\ = {} & \frac{-a^2}{\pi j\,\sqrt{1-w^2}}\int_{-\infty}^{\infty}\int_{-\infty}^{\infty}\frac{e^{j(\xi^2+2w\xi\eta+\eta^2)}}{\xi^2-\frac{a^2}{1-w^2}}\,d\xi\,d\eta \\ = {} & F(a^2) \end{aligned} \tag{40}$$

where F is the UTD transition function in (20).

ACKNOWLEDGMENT

The authors wish to express their appreciation to Prof. L. B. Felsen for useful and stimulating discussions.

REFERENCES

[1] R. G. Kouyoumjian and P. H. Pathak, "A uniform geometrical theory of diffraction for an edge in a perfectly conducting surface," *Proc. IEEE*, vol. 62, pp. 1448–1461, Nov. 1974.
[2] L. B. Felsen and L. Carin, "Frequency and time domain Bragg-modulated acoustic for truncated periodic array," *J. Acoust. Soc. Amer.*, Feb. 1994.
[3] ———, "Diffraction theory of frequency and time domain scattering by weakly aperiodic truncated thin wire gratings," *J. Opt. Soc. Amer.*, Feb. 1994.
[4] L. Carin and L. B. Felsen, "Time harmonic and transient scattering by finite periodic flat strip arrays: Hybrid ray–Floquet mode-MoM algorithm," *IEEE Trans. Antennas Propagat.*, vol. 41, pp. 412–421, Apr. 1993.
[5] L. Carin, L. B. Felsen, and T.-T. Hsu, "High-frequency fields excited by truncated arrays of nonuniformly distributed filamentary scatterers on an infinite dielectric grounded slab: Parametrizing leaky mode-Floquet mode interaction," *IEEE Trans. Antennas Propagat.*, vol. 44, pp. 1–11, Jan. 1996.
[6] F. Capolino, M. Albani, S. Maci, and R. Tiberio, "Diffraction from a couple of coplanar, skew wedges," *IEEE Trans. Antennas Propagat.*, vol. 45, pp. 1219–1226, Aug. 1997.
[7] M. Albani, F. Capolino, S. Maci, and R. Tiberio, "Diffraction at a thick screen including corrugations on the top face," *IEEE Trans. Antennas Propagat.*, vol. 45, Feb. 1997.
[8] F. Capolino and S. Maci, "Uniform high-frequency description of singly, doubly, and vertex diffracted rays for a plane angular sector," *J.E.M. Wave and Appl.*, Oct. 1996.
[9] L. B. Felsen and N. Marcuvitz, *Radiation and Scattering of Waves.* Englewood Cliffs, NJ: Prentice-Hall, 1973.
[10] B. L. Van der Waerden, "On the method of saddle points," *Appl. Sci. Res.*, vol. B2, pp. 33–45, 1951.
[11] H. Bertoni, A. C. Green, and L. B. Felsen, "Shadowing on inhomogeneous plane wave by an edge," *J. Opt. Soc. Amer.*, July 1978.
[12] F. Capolino, M. Albani, A. Neto, S. Maci, and L. B. Felsen, "Vertex-diffracted Floquet waves at a corner array of dipoles," in *Proc. Int. Conf. Electromagnetics in Advanced Applications (ICEAA)*, Torino, Italy, Sept. 16–18, 1997.
[13] A. Neto, S. Maci, M. Sabbadini, and G. Vecchi, "Edge fringe approach for the full-wave solution of large finite arrays," in *Proc. Antennas and Propagation Symp.*, Montreal, Ont., Canada, July 13–18, 1997.
[14] D. S. Jones, "A uniform asymptotic expansion for a certain double integral," in *Proc. Roy. Soc. Edin. (A)*, 1971, vol. 69, pp. 205–226.
[15] F. Capolino and S. Maci, "Simplified, closed-form expressions for computing the generalized Fresnel integral and their application to vertex diffraction," *Microwave Opt. Technol. Lett.*, vol. 9, no. 1, pp. 32–37, May 1995.

Filippo Capolino (S'94–M'97) was born in Florence, Italy, in 1967. He received the doctor degree (*cum laude*) in electronic engineering and the Ph.D. degree both from the University of Florence, Italy, in 1993 and 1997, respectively.

From 1994 to 1996, he was an Instructor at the University of Siena, where he is currently a Research Assistant. His research interests include theoretical and applied electromagnetics, focused on high-frequency methods for electromagnetic scattering, and electromagnetic models of random surfaces.

Dr. Capolino received a MMET 1994 Student Paper Competition Award, the Raj Mittra Travel Grant for Young Scientists in 1996, and the "Barzilai" Prize for the Best Paper at the National Italian Congress of Electromagnetism (XI RiNEm).

Matteo Albani (M'95) was born in Florence, Italy, in 1970. He received the doctor degree (*cum laude*) in electronic engineering from the University of Florence, Italy. He is currently working toward the Ph.D. degree at the University of Siena.

His research interests include numerical methods for electromagnetics.

Dr. Albani received a special award for his Laurea thesis work from the University of Florence.

Stefano Maci (M'92) was born in Rome, Italy, in 1961. He received the doctor degree in electronic engineering from the University of Florence, Italy, in 1987.

In 1990, he joined the Department of Electronic Engineering of the University of Florence as an Assistant Professor. Since 1993, he has been also an Adjunct Professor at the University of Siena, Italy. In 1997, he was an invited Professor at the Technical University of Denmark, Copenhagen. His interests include electromagnetic theory, mainly concerning high- and low-frequency methods for antennas and electromagnetic scattering. He has also developed research activity on specific topics concerning microwaves antennas, particularly focused on the analysis, synthesis and design of patch antennas. Since 1996, he has been involved in projects of the European Space Agency regarding electromagnetic modeling.

Dr. Maci received the National Young Scientists "Francini" Award for the Laurea thesis in 1988 and the "Barzilai" Prize for the Best Paper at the National Italian Congress of Electromagnetism (XI RiNEm) in 1996.

Roberto Tiberio (M'81–SM'83–F'93) was born in Rome in 1946. He received the doctor degree (*cum laude*) in 1970 from the University of Pisa, Italy.

In 1972, he joined the Department of Electronic Engineering of the University of Florence, where he was a Full Professor until October 1993. Next, he joined the University of Siena, where he has been the Dean of the College of Engineering. Since 1976, he has been collaborating with the Electroscience Laboratory of the Ohio State University, Columbus, OH, where he worked continuously as a Senior Research Assistant for two years and then periodically as a Scientific Consultant. His research interests include the electromagnetic theory and high-frequency methods, mainly concerning the development and applications of analytic and numerical techniques for antenna design and radar cross section prediction.

Dr. Tiberio is an Italian Delegate of URSI (Commission B).